**Proceedings of the ASME 2012 International Design Engineering Technical Conferences & Computers and Information in Engineering Conference**
**IDETC/CIE 2012**
**August 12-15, 2012, Chicago, IL, USA**

# DETC2012-70467

# MODELING SLOPE DISCONTINUITY OF LARGE SIZE WIND-TURBINE BLADE USING ABSOLUTE NODAL COORDINATE FORMULATION

**Ahmed H. Bayoumy**
Faculty of Engineering
Cairo University, Egypt.
a.hamdy85@ymail.com

**Ayman A. Nada***
College of Engineering,
Jazan University, KSA.
anada@jazanu.edu.sa

**Said M. Megahed**
Faculty of Engineering
Cairo University, Egypt.
smegahed@cu.edu.eg

## ABSTRACT

*This paper describes the use of the Absolute Nodal Coordinate Formulation (ANCF) in modeling large-size wind turbine blades. An efficient procedure is developed for mapping NACA airfoil wind-turbine blades into ANCF thin plate models. The procedure concerns the wind turbine blade with non-uniform, twisted nature. As a result, the slope discontinuity problem arises and presents numerical errors in the dynamic simulation. This investigation illustrates a method for modeling slope discontinuity resulting from the variations of the cross sectional layouts across the blade. A method is developed and applied for the gradient-deficient thin plate element in order to account for structural discontinuity. The numerical results show a numerical convergence and satisfy the principle of work and energy in dynamics. The simulation results are compared with those obtained using ANSYS code with a good agreement.*

## NOMENCLATURE

- $a$ Length of plate in initial configuration(m)
- $\alpha$ Taper angle of WTB (rad)
- $b$ Width of plate in initial configuration(m)
- $\mathbf{B}_1$ Connectivity matrix
- $\mathbf{B}_2$ Boundary condition matrix
- $c$ Chord length (parametric)
- $\mathbf{e}$ Vector of absolute nodal coordinates
- $h$ Maximum thickness of airfoil (parametric)
- $\eta$ Parametric position along $y-$axis
- $\mathbf{I}$ Identity matrix
- $L_s$ Span length of wind turbine blade(m)
- $m$ Maximum camber (parametric)
- $p$ Maximum camber location (parametric)
- $\mathbf{p}$ Vector of unconstrained nodal coordinates
- $\mathbf{r}$ Position vector in the global coordinate system
- $\mathbf{r}_x$ Longitudinal gradient vector
- $\mathbf{r}_y$ Transverse gradient vector
- $\mathbf{S}$ Shape function matrix
- $t$ Thickness of plate element(m)
- $\mathbf{u}$ Local position vector
- $\mathbf{x}$ Vector of local coordinates $(x,y,z)$
- $\mathbf{X}$ Vector of global coordinates $(X,Y,Z)$
- $\xi$ Parametric position along $x-$axis
- $z_c$ Camber line position coordinates $z-$axis (parametric)
- $z_{th}$ Thickness distribution of the NACA airfoil (parametric)

**Keywords**: ANCF, WTB, Plate element, Slope discontinuity.

## INTRODUCTION

In recent years the aerodynamic performance of wind turbine blades has been improved considerably. The energy capture increases with the square of the length of the blades [1]. However, the weight of the blade increases with the cube of the length of the blade [1]. To counteract the weight increase the development of blades goes towards long and relatively flexible structures.The most important aeroelastic components of a

*On leave, Benha Institute of Technology, Benha University, Benha, Egypt.

**FIGURE 1**. REAL PICTURE OF LARGE SIZE WIND TURBINE BLADE

wind turbine are the blades. The purpose of the blades is to extract aerodynamic forces from the passing airflow, therefore they are highly affected by aerodynamic forces. Furthermore the development of larger wind turbines has resulted in long slender blades with high flexibility. The modeling problem increases as the rotor blade diameter increases, for instance, a wind turbine, at Risoe National Laboratory, Denmark [2] has a tower height of $(120m)$, rotor diameter of $(110m)$, see Fig.1. A good literature of wind turbine modeling methods may be found in [3,4].

The recently developed ANCF has been used in the analysis of large deformation of flexible multibody systems include belt drives [5–7], rotor blade [8], piezo-electric laminated plates [9], flexible manipulators [10], and cable applications [11]. The important advantage of using this formulation in multibody computer simulations is the obtained constant mass matrix, which can be obtained fully nonlinear dynamic problems. Therefore, this non-linear finite element formulation can be implemented using non-incremental solution procedures in a general framework of multibody computer algorithms. The elastic forces, in contrast, are calculated using a general continuum mechanics approach that allows for describing the cross-section deformation modes as well as the deformation modes that appear in the existing beam theories. Recent advances in ANCF, involving the method of calculating the strain energy [12], illuminating high frequency modes [13, 14], development of stiff integrators [15, 16] help in reducing the calculation time and enhance the sensitivity of the system equations. Also the formulation of 3D joint constraints is well established and verified [17], which enable to construct the model of complete wind turbine blades and structure. Further advances in the ANCF are carried out including the modeling of internal damping [18] and nonlinear viscoelasticity [19].

The desirable features of the ANCF mentioned above remain in effect even in the case of flexible bodies with slope discontinuities [20]. As demonstrated in the literature [20], fully parameterized ANCF elements, which have a complete set of gradient vectors (beam and thick plate), can be used to model slope discontinuities in a straight forward manner. In the case of gradient deficient elements, which employ a reduced set of parameters (thin beam, thin plate), do not have a complete set of gradient vectors. The difficulties associated using these gradient deficient ANCF finite elements in modeling slope discontinuities have been discussed for thin beams in [21,22] and for certain kind of rotations in [23,24]. General methods for modeling slope discontinuities of gradient deficient elements are discussed in [25].

In this paper, an ANCF model of large-size wind turbine blade is developed using thin plate elements. The use of the thin plate element is more efficient in that application because of the relative scale between the thickness and length and width. A procedure of constructing the ANCF model of NACA airfoils of wind turbine blades is established. Because of the variations of the cross sectional layouts across the blade, structural discontinuities are found between the upper and lower surfaces and between the blade body and root-blade section. The paper suggest a method of modeling the slope discontinuities of the finite element model of the wind turbine blade. Numerical examples are carried out with good agreement with ANSYS code results.

## ABSOLUTE NODAL COORDINATE FORMULATION

In the absolute nodal coordinate formulation, the nodal coordinates of the elements are defined in a fixed inertial coordinate system, this fixed inertial coordinate system should be mentioned here as the Structure Coordinate System **SCS:**$(XYZ)$. The nodal coordinates of an element $j$ are consisting of the global displacements and slopes of each node. For a 4-noded plate element, element $j$, on body $i$, as shown in Fig.2, the nodal coordinates of node $k$, $k=(1,2,3,4)$ can be written as:

$$\mathbf{e}^{ijk}=\left[\mathbf{r}^{ijk^T}\ \frac{\partial \mathbf{r}^{ijk}}{\partial x^{ij}}^T\ \frac{\partial \mathbf{r}^{ijk}}{\partial y^{ij}}^T\ \frac{\partial \mathbf{r}^{ijk}}{\partial z^{ij}}^T\right]^T \tag{1}$$

where $\mathbf{r}^{ijk}$ defines the global position of node $k$ and the three vectors $\partial\mathbf{r}^{ijk}/\partial x^{ij}$, $\partial\mathbf{r}^{ijk}/\partial y^{ij}$, and $\partial\mathbf{r}^{ijk}/\partial z^{ij}$, define the position vector gradients at node $k$ with respect to the element coordinate system **ECS:**$\left(x^{ij},y^{ij},z^{ij}\right)$. As a consequence, such a representation guarantees inter-element continuity of global displacement gradients at these points. The nodal coordinates of one element can then be given by the vector $\mathbf{e}^{ij}=\left[\mathbf{e}^{ij1T}\ \mathbf{e}^{ij2T}\ \mathbf{e}^{ij3T}\ \mathbf{e}^{ij4T}\right]^T$. In the ANCF, the global position of an arbitrary point on the body $i$, element $j$, is defined as:

$$\mathbf{r}^{ij} = \mathbf{S}^{ij}\left(\mathbf{u}^{ij}\right)\mathbf{e}^{ij} \tag{2}$$

where $\mathbf{S}^{ij}$ is the element shape function matrix [26], $\mathbf{u}^{ij} = \left[x^{ij}\ y^{ij}\ z^{ij}\right]^T$ is the local position of the point, $x^{ij}, y^{ij}$ and $z^{ij}$ are the local coordinates of the element defined in the **ECS.** By defining $\mathbf{p}^i$ as the *unconstrained* vector of nodal coordinates over the flexible body $i$, with the dimension of $DOFs \times 1$, where $DOFs$ are the total number of degrees of freedom. Thus, Eqn.(2) can be rewritten as:

$$\mathbf{r}^{ij} = \mathbf{S}^{ij}\mathbf{e}^{ij} = \mathbf{S}^{ij}\mathbf{B}_1^{ij}\mathbf{B}_2^{i}\mathbf{p}^{i} \tag{3}$$

where $\mathbf{B}_1^{ij}$ is the connectivity matrix and $\mathbf{B}_2^{i}$ is boundary conditions linear-transformation matrix.

## Slope Discontinuity

Assuming that the element has an arbitrary initial orientation, see Fig.3, $\mathbf{r}^{ij}$ can be defined using the **ECS** as follows:

$$\mathbf{r}^{ij} = \mathbf{R}^{ij} + \mathbf{A}^{ij}\mathbf{u}^{ij} \tag{4}$$

where $\mathbf{R}^{ij}$ is the global position vector of the origin of the element coordinate system, and $\mathbf{A}^{ij}$ is the transformation matrix that defines the orientation of the **ECS** with respect to the **SCS**. Therefore the position vector gradients with respect to the **ECS** in the initial configuration can be obtained as:

$$\frac{\partial \mathbf{r}^{ij}}{\partial \mathbf{u}^{ij}} = \mathbf{A}^{ij} \tag{5}$$

To maintain the desirable features of the ANCF that include a constant mass matrix and zero Coriolis and centrifugal forces; it is provided that all the element transformation matrices that defines the orientation of the **ECS** with respect to **SCS** are the same. That is if two elements have initially different orientations; the continuity of the position vector gradients can not be maintained, consequently, this leads to a nonlinear mass matrix for the flexible body. In order to model slope discontinuities in such away to lead to constant mass matrix for the element that undergoes finite rotation and large deformation, an intermediate coordinate system is introduced [20], in which a body-parameterization is used instead of the element parameterization. This intermediate coordinate system is mentioned in this investigation by the body coordinate system **BCS**. If the axes of the **BCS** is selected to be initially parallel to the axes of the **SCS**, as shown in Fig.3, Eqn.(4) should take the form of:

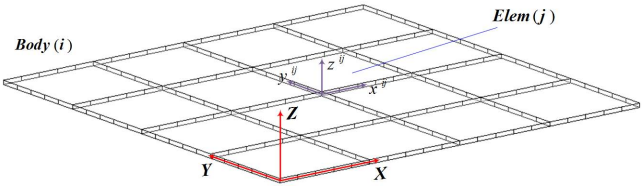


**FIGURE 2**. UN-DEFORMED CONFIGURATION OF PLATE ELEMENT

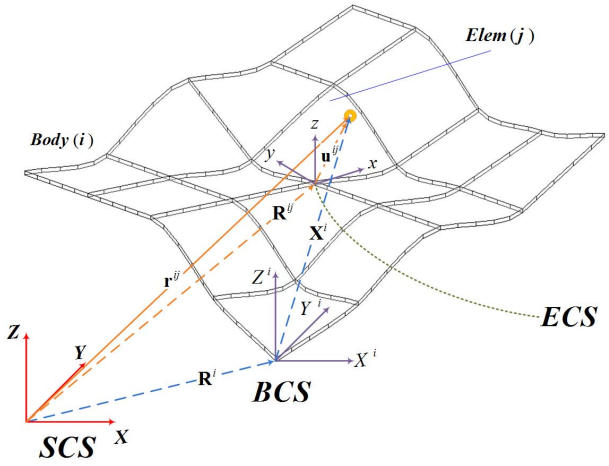


**FIGURE 3**. STRUCTURE (SCS), BODY (BCS) AND ELEMENT (ECS) COORDINATE SYSTEMS OF CONTINUOUS STRUCTURE

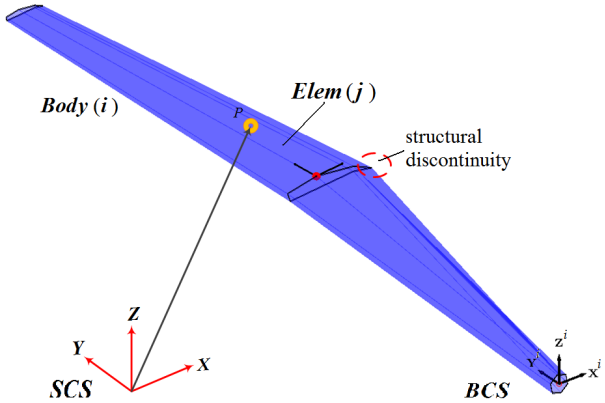


**FIGURE 4**. STRUCTURE (SCS), BODY (BCS) AND ELEMENT (ECS) COORDINATE SYSTEMS OF DISCONTINUOUS STRUCTURE

$$\mathbf{r}^{ij} = \mathbf{R}^{i} + \mathbf{X}^{i} \tag{6}$$

where $\mathbf{R}^i$ is the global position vector of the origin of the body coordinate system, and $\mathbf{X}^i = \begin{bmatrix} X^i & Y^i & Z^i \end{bmatrix}$ are the body parameterization. Therefore, the position vector gradients for all the elements over the body $i$,can be obtained as:

$$\frac{\partial \mathbf{r}^{ij}}{\partial \mathbf{X}^i} = \mathbf{I} \tag{7}$$

where $\mathbf{I}$ is a $3 \times 3$ identity matrix. This means that, using the **BCS**, all the position vector gradients of all elements are the same and consequently a standard ANCF assembly can be established. The gradients transformation between the **BCS** and the **ECS** can be written as [25]:

$$\begin{bmatrix} \mathbf{r}_{x^{ij}}^{ij} & \mathbf{r}_{y^{ij}}^{ij} & \mathbf{r}_{z^{ij}}^{ij} \end{bmatrix} = \begin{bmatrix} \mathbf{r}_{X^i}^{ij} & \mathbf{r}_{Y^i}^{ij} & \mathbf{r}_{Z^i}^{ij} \end{bmatrix} \begin{bmatrix} \frac{\partial X^i}{\partial x^{ij}} & \frac{\partial Y^i}{\partial x^{ij}} & \frac{\partial Z^i}{\partial x^{ij}} \\ \frac{\partial X^i}{\partial y^{ij}} & \frac{\partial Y^i}{\partial y^{ij}} & \frac{\partial Z^i}{\partial y^{ij}} \\ \frac{\partial X^i}{\partial z^{ij}} & \frac{\partial Y^i}{\partial z^{ij}} & \frac{\partial Z^i}{\partial z^{ij}} \end{bmatrix} \tag{8}$$

Simply, Eqn.(8) can be rewritten as: $\mathbf{r}_{\mathbf{x}^{ij}}^{ij} = \mathbf{J}_0^{ijT} \mathbf{r}_{\mathbf{X}^i}^{ij}$, where $\mathbf{J}_0$ is the orthogonal transformation matrix that describe the initial orientation of the **ECS** with respect to **BCS** and can be written in the form of:

$$\mathbf{J}_0^j = \begin{bmatrix} J_{0(1,1)}^j & J_{0(1,2)}^j & J_{0(1,3)}^j \\ J_{0(2,1)}^j & J_{0(2,2)}^j & J_{0(2,3)}^j \\ J_{0(3,1)}^j & J_{0(3,2)}^j & J_{0(3,3)}^j \end{bmatrix} \tag{9}$$

Thus, the element coordinate transformation of the nodal point $k$ can be carried out using the following equations:

$$\begin{bmatrix} \mathbf{r}^{ijk} \\ \mathbf{r}_{x^{ij}}^{ijk} \\ \mathbf{r}_{y^{ij}}^{ijk} \\ \mathbf{r}_{z^{ij}}^{ijk} \end{bmatrix} = \begin{bmatrix} \mathbf{I} & \mathbf{0} & \mathbf{0} & \mathbf{0} \\ \mathbf{0} & J_{0(1,1)}^{ijk}\mathbf{I} & J_{0(2,1)}^{ijk}\mathbf{I} & J_{0(3,1)}^{ijk}\mathbf{I} \\ \mathbf{0} & J_{0(1,2)}^{ijk}\mathbf{I} & J_{0(2,2)}^{ijk}\mathbf{I} & J_{0(3,2)}^{ijk}\mathbf{I} \\ \mathbf{0} & J_{0(1,3)}^{ijk}\mathbf{I} & J_{0(2,3)}^{ijk}\mathbf{I} & J_{0(3,3)}^{ijk}\mathbf{I} \end{bmatrix} \begin{bmatrix} \mathbf{r}^{ijk} \\ \mathbf{r}_X^{ijk} \\ \mathbf{r}_Y^{ijk} \\ \mathbf{r}_Z^{ijk} \end{bmatrix} \tag{10}$$

$$\mathbf{e}^{ijk} = \mathbf{T}^{ijk}\mathbf{P}^{ijk} \tag{11}$$

where $\mathbf{P}^{ijk} = \begin{bmatrix} \mathbf{r}^{ijk} & \mathbf{r}_X^{ijkT} & \mathbf{r}_Y^{ijkT} & \mathbf{r}_Z^{ijkT} \end{bmatrix}^T$, thus, Eqn.(3) can be modified into:

$$\mathbf{r}^{ij} = \mathbf{S}^{ij}\mathbf{T}^{ij}\mathbf{B}_1^{ij}\mathbf{B}_2^i\mathbf{P}^i \tag{12}$$

This allows maintaining the ANCF desirable features that include a constant mass matrix and zero Coriolis and centrifugal forces in the equations of motion of structures that experience arbitrary large displacements.

### Gradient Deficient Elements

In the case of slope discontinuity of gradient deficient ANCF finite elements as the case of thin plates, Eqn.(10) reduces to:

$$\begin{bmatrix} \mathbf{r}^{ijk} \\ \mathbf{r}_{x^{ij}}^{ijk} \\ \mathbf{r}_{y^{ij}}^{ijk} \end{bmatrix} = \begin{bmatrix} \mathbf{I} & \mathbf{0} & \mathbf{0} & \mathbf{0} \\ \mathbf{0} & J_{0(1,1)}^{ijk}\mathbf{I} & J_{0(2,1)}^{ijk}\mathbf{I} & J_{0(3,1)}^{ijk}\mathbf{I} \\ \mathbf{0} & J_{0(1,2)}^{ijk}\mathbf{I} & J_{0(2,2)}^{ijk}\mathbf{I} & J_{0(3,2)}^{ijk}\mathbf{I} \end{bmatrix} \begin{bmatrix} \mathbf{r}^{ijk} \\ \mathbf{r}_X^{ijk} \\ \mathbf{r}_Y^{ijk} \\ \mathbf{r}_Z^{ijk} \end{bmatrix} \tag{13}$$

One can always define at the element interface three independent structure coordinate lines that lie on the structure surface [25]. In this investigation, thin plate elements are used to model the large size wind turbine blades, see Fig.4. The use of thin plate element in modeling the wind turbine plate is obvious because of the large relative size between the plate thickness and the plate length and width. Structural discontinuity in this case is apparent along the blade length and therefore, Eqn.(13) should be used properly. It is important, however, to point out that, fully parameterized elements with efficient elastic force formulations can always be used if necessary instead of gradient deficient elements.

## AIRFOIL SHAPE PARAMETERS

Wind turbines on the propeller blades possess various blade profiles such as NACA, LS and LM profiles standards [27]. In horizontal axis wind turbines NACA profiles standards of **N**ational **A**dvisory **C**ommittee for **A**eronautics is applied [28]. The shape of the airfoil can be chosen in the famous NACA 4 digits library [28]. This simple library is interesting because the shape is expressed analytically as a function of three parameters, which control the maximum camber, maximum camber location, and maximum thickness of the airfoil, see Fig.5.
The camber line can be expressed in the $xz$ plane, as:

$$\frac{z_c}{c} = \frac{m}{p^2}\left(2p\xi - \xi^2\right), \cdots \xi \leq p \tag{14}$$

$$= \frac{m}{(1-p)^2}\left(1 - 2p + 2p\xi - \xi^2\right), \xi \geq p \tag{15}$$

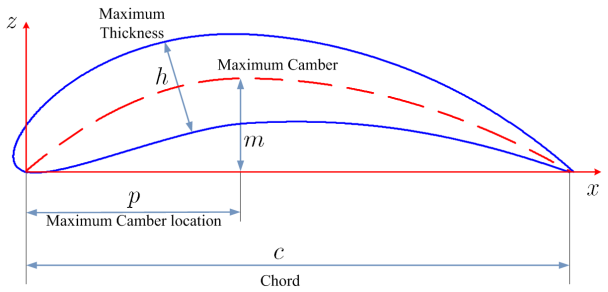


**FIGURE 5**. AIRFOIL SHAPE PARAMETERS

In these expressions, $c$ is the airfoil chord length, $m$ is the maximum camber, $p$ is the maximum camber location, and $\xi = (x/c)$ is the *parametric position.* The thickness distribution for the NACA 4-digits sections is given by:

$$z_{th} = 5ch(0.2969\,\xi^{1/2} - 0.1260\,\xi - 0.3516\xi^2 + 0.2843\,\xi^3 - 0.1015\,\xi^4) \tag{16}$$

where $h$ is the maximum thickness expressed as a fraction of the chord. The wing section is obtained by combining the camber line and the thickness distribution as described by:

$$\left.\begin{aligned} x_u &= x - z_{th}\sin\theta \\ z_u &= z_c + z_{th}\cos\theta \\ x_l &= x + z_{th}\sin\theta \\ z_l &= z_c - z_{th}\cos\theta \end{aligned}\right\} \tag{17}$$

Here, $\theta$ is the slope of the camber line, and can be calculated using the following equation:

$$\frac{dz_c}{dx} = \frac{d(z_c/c)}{d\xi} = \frac{2m}{p^2}(p-\xi), \cdots \xi \le p \tag{18}$$

$$= \frac{d(z_c/c)}{d\xi} = \frac{2m}{(1-p)^2}(p-\xi), \xi \ge p \tag{19}$$

## ANCF Model of Uniform Wind Turbine Blade

The blade profile is a hollow profile usually formed by two structures glued together, one upper shell on the suction side, and one lower shell on the pressure side. It is required to construct the wind turbine blade with specific NACA code, and therefore, the NACA profile equations should be used to estimate the nodal position and nodal gradients. In this section, ANCF thin plate element should be used to construct the wind turbine blade. It is found that six elements can be used to construct the blade model in such away to coincide with the NACA code. The NACA thickness distribution, Eqn.(17) should be used to estimate the nodal position and gradients along the chord length. Three plate elements are used for the upper surface and three others for the lower side of the wind turbine blade. The construction procedure is tabulated in Tab.(1) and Tab.(2). The tables show the statements of the nodal coordinates,i.e., nodal position and gradients of the upper and lower surfaces respectively. Figure (6) shows the nodes and the corresponding gradients of each node, as described in Tab.(1,2).

**TABLE 1**. STATEMENTS OF NODAL COORDINATES OF THE UPPER SURFACE

| $k$ | $x$ | $\mathbf{r}^k$ | $\mathbf{r}^k_x$ | $\mathbf{r}^k_y$ |
|---|---|---|---|---|
| 1 | $0.1c$ | $\begin{bmatrix} x_u & 0 & z_u \end{bmatrix}^T$ | $\begin{bmatrix} \frac{dx_u}{dx} & 0 & \frac{dz_u}{dx} \end{bmatrix}^T$ | $\begin{bmatrix} 0 & 1 & 0 \end{bmatrix}^T$ |
| 2 | $p$ | $\begin{bmatrix} x_u & 0 & z_u \end{bmatrix}^T$ | $\begin{bmatrix} \frac{dx_u}{dx} & 0 & \frac{dz_u}{dx} \end{bmatrix}^T$ | $\begin{bmatrix} 0 & 1 & 0 \end{bmatrix}^T$ |
| 3 | $p$ | $\begin{bmatrix} x_u & L_s & z_u \end{bmatrix}^T$ | $\begin{bmatrix} \frac{dx_u}{dx} & 0 & \frac{dz_u}{dx} \end{bmatrix}^T$ | $\begin{bmatrix} 0 & 1 & 0 \end{bmatrix}^T$ |
| 4 | $0.1c$ | $\begin{bmatrix} x_u & L_s & z_u \end{bmatrix}^T$ | $\begin{bmatrix} \frac{dx_u}{dx} & 0 & \frac{dz_u}{dx} \end{bmatrix}^T$ | $\begin{bmatrix} 0 & 1 & 0 \end{bmatrix}^T$ |
| 5 | $c$ | $\begin{bmatrix} x_u & 0 & z_u \end{bmatrix}^T$ | $\begin{bmatrix} \frac{dx_u}{dx} & 0 & \frac{dz_u}{dx} \end{bmatrix}^T$ | $\begin{bmatrix} 0 & 1 & 0 \end{bmatrix}^T$ |
| 6 | $c$ | $\begin{bmatrix} x_u & L_s & z_u \end{bmatrix}^T$ | $\begin{bmatrix} \frac{dx_u}{dx} & 0 & \frac{dz_u}{dx} \end{bmatrix}^T$ | $\begin{bmatrix} 0 & 1 & 0 \end{bmatrix}^T$ |
| 13 | 0 | $\begin{bmatrix} x_u & 0 & z_u \end{bmatrix}^T$ | $\begin{bmatrix} 0 & 0 & 1 \end{bmatrix}^T$ | $\begin{bmatrix} 0 & 1 & 0 \end{bmatrix}^T$ |
| 14 | 0 | $\begin{bmatrix} x_u & L_s & z_u \end{bmatrix}^T$ | $\begin{bmatrix} 0 & 0 & 1 \end{bmatrix}^T$ | $\begin{bmatrix} 0 & 1 & 0 \end{bmatrix}^T$ |

**TABLE 2**. STATEMENTS OF NODAL COORDINATES OF THE LOWER SURFACE

| $k$ | $x$ | $\mathbf{r}^k$ | $\mathbf{r}^k_x$ | $\mathbf{r}^k_y$ |
|---|---|---|---|---|
| 7 | $0.055c$ | $\begin{bmatrix} x_l & 0 & z_l \end{bmatrix}^T$ | $\begin{bmatrix} \frac{dx_l}{dx} & 0 & \frac{dz_l}{dx} \end{bmatrix}^T$ | $\begin{bmatrix} 0 & 1 & 0 \end{bmatrix}^T$ |
| 8 | $p$ | $\begin{bmatrix} x_l & 0 & z_l \end{bmatrix}^T$ | $\begin{bmatrix} \frac{dx_l}{dx} & 0 & \frac{dz_l}{dx} \end{bmatrix}^T$ | $\begin{bmatrix} 0 & 1 & 0 \end{bmatrix}^T$ |
| 9 | $p$ | $\begin{bmatrix} x_l & L_s & z_l \end{bmatrix}^T$ | $\begin{bmatrix} \frac{dx_l}{dx} & 0 & \frac{dz_l}{dx} \end{bmatrix}^T$ | $\begin{bmatrix} 0 & 1 & 0 \end{bmatrix}^T$ |
| 10 | $0.055c$ | $\begin{bmatrix} x_l & L_s & z_l \end{bmatrix}^T$ | $\begin{bmatrix} \frac{dx_l}{dx} & 0 & \frac{dz_l}{dx} \end{bmatrix}^T$ | $\begin{bmatrix} 0 & 1 & 0 \end{bmatrix}^T$ |
| 11 | $c$ | $\begin{bmatrix} x_l & 0 & z_l \end{bmatrix}^T$ | $\begin{bmatrix} \frac{dx_l}{dx} & 0 & \frac{dz_l}{dx} \end{bmatrix}^T$ | $\begin{bmatrix} 0 & 1 & 0 \end{bmatrix}^T$ |
| 12 | $c$ | $\begin{bmatrix} x_l & L_s & z_l \end{bmatrix}^T$ | $\begin{bmatrix} \frac{dx_l}{dx} & 0 & \frac{dz_l}{dx} \end{bmatrix}^T$ | $\begin{bmatrix} 0 & 1 & 0 \end{bmatrix}^T$ |
| 15 | 0 | $\begin{bmatrix} x_l & 0 & z_l \end{bmatrix}^T$ | $\begin{bmatrix} 0 & 0 & -1 \end{bmatrix}^T$ | $\begin{bmatrix} 0 & 1 & 0 \end{bmatrix}^T$ |
| 16 | 0 | $\begin{bmatrix} x_l & L_s & z_l \end{bmatrix}^T$ | $\begin{bmatrix} 0 & 0 & -1 \end{bmatrix}^T$ | $\begin{bmatrix} 0 & 1 & 0 \end{bmatrix}^T$ |

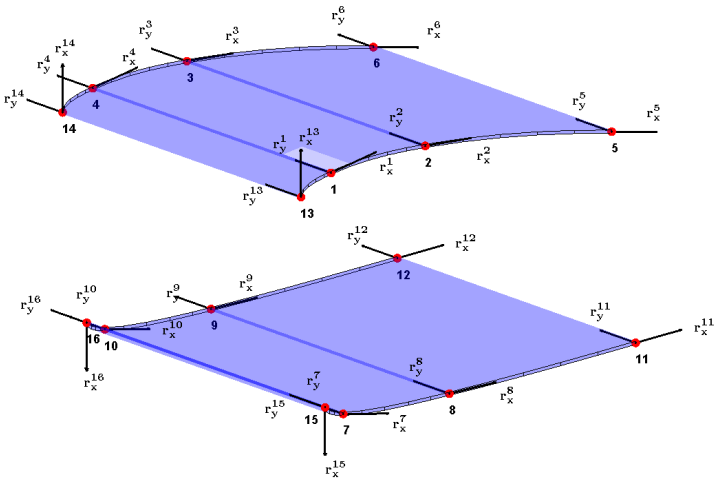

**FIGURE 6**. NODAL POSITIONS AND GRADIENTS

It is clear that, structural discontinuity appears at the interface sections. Points number (13,14) on the upper surface and points (15,16) on the lower surface at the leading edge of the blade have different gradients in the $x-$axis. Also, points number (5,6) on the upper surface and points (11,12) on the lower surface at the trailing edge of the blade have different gradients along the $x-$axis. While the geometric construction of the wind turbine blade is carried out successfully, see Fig.7, the structural discontinuity prevents the elements assembly process for correct dynamic simulation.

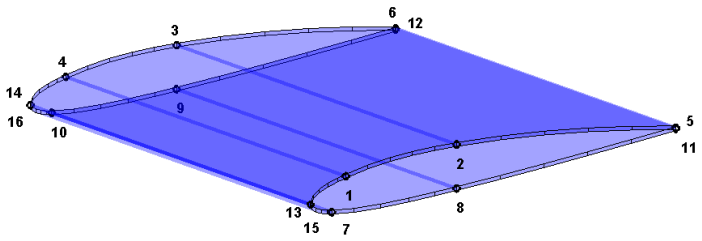

**FIGURE 7**. DISCONTINUOUS ANCF MODEL OF WTB

## ANCF Model of Non-Uniform Wind Turbine Blade

It is important that the blade sections near the hub are able to resist forces and stresses from the rest of the blade. Therefore, the blade profile near the root is both thick and wide. Further, along the blade, the blade profile becomes thinner so as to obtain acceptable aerodynamic properties. Therefore, the effect of tapering the blade is obvious; it tends to decrease the stresses. The design process of the blade constitutes a compromise between the desire for strength and the desire for good aerodynamic properties. At the root, the blade profile is usually narrower and tubular to fit the hub. From the geometric point of view, tapering is connecting two cross sections along the span length, $L_s$, within the blade surface, with an angle called the taper angle, $\alpha$; the change in the chord length, $\Delta c$, can be obtained as:

$$\Delta c = L_s \tan\alpha \Leftrightarrow c_2 = c_1 - \Delta c \tag{20}$$

where $c$ is the chord length, and $c_1$, $c_2$ are the chord length at the 'start' and 'tip' cross sections respectively. In this investigation, the lofted surface goemetry [29] is used to construct the ANCF model of the tapered (non-uniform) blade. The lofted surface is constructed between the 'start' and the 'tip' cross sections. In the case of obtaining the global position vector for the non-uniform wind turbine blade; the position vector $\mathbf{r}$ should be linearly interpolated between the blade starting chord and the ending chord. This bounded curves can be denoted by $\mathbf{r}(\xi,0)$ and $\mathbf{r}(\xi,1)$ and by two straight segments $\mathbf{r}(0,\eta)$ and $\mathbf{r}(1,\eta)$ connecting them. Surface lines in $\eta$ direction are therefore straight,i.e., lofted surfaces, whereas each line in the $\xi$ direction is a blend of $\mathbf{r}(\xi,0)$ and $\mathbf{r}(\xi,1)$ this blend constitutes the surface expression of:

$$\mathbf{r}(\xi,\eta) = (1-\eta)\,\mathbf{r}(\xi,0) + \eta\,\mathbf{r}(\xi,1) \tag{21}$$

where $\eta$ and $\xi$ are parametric domains such that $\xi,\eta \in [0,1]$ and can be estimated as $\xi = x/a, \eta = y/b$, with $a$, and $b$ are the plate element length and width respectively. It should be mentioned here that this kind of surface is fully defined by specifying the two boundary curves. The four corner points of the plate elements are implicit in these curves. Depending on $c_1$ and $c_2$, the boundary curves can be obtained as:

$$\mathbf{r}(\xi,0) = \mathbf{r}^i = \mathbf{S}(x,0)\,\mathbf{e} \quad \cdots, x \in [0, c_1] \tag{22}$$

where $\mathbf{e}$ is the nodal coordinates of the starting cross section $i$. Thus, the position vector at the end cross section can be concluded as:

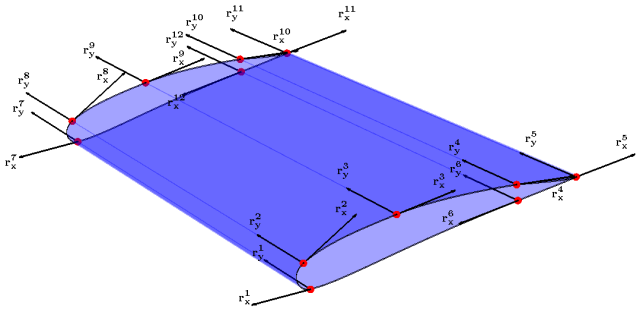

**FIGURE 8**. CONSTRUCTION OF TAPERED BLADES (START-END SECTION)

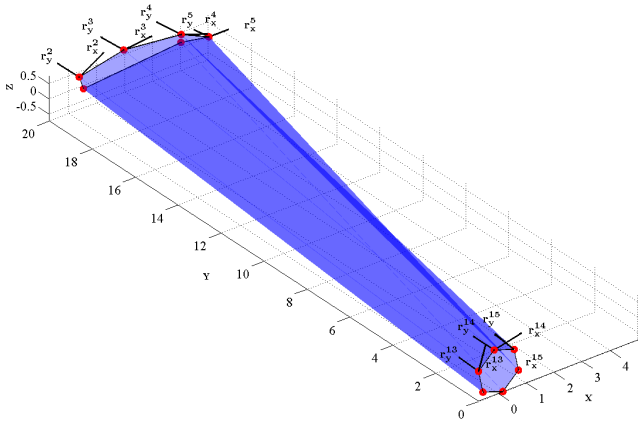

**FIGURE 9**. CONSTRUCTION OF TAPERED BLADES (ROOT-BLADE SECTION)

$$\mathbf{r}(\xi,1) = \mathbf{r}^j = \begin{bmatrix} 0 \\ L_s \\ 0 \end{bmatrix} + \begin{bmatrix} \frac{c_2}{c_1} & 0 & 0 \\ 0 & 1 & 0 \\ 0 & 0 & \frac{c_2}{c_1} \end{bmatrix} \mathbf{r}(\xi,0) \qquad (23)$$

By substituting Eqn.(22 , 23) into Eqn.(21) gives the curves of cross sections between $\mathbf{r}^i$ and $\mathbf{r}^j$. Then, Eqn.(21) can be solved for the nodal coordinates $\mathbf{e}$ of the ending cross section. i.e., the nodal coordinates of nodes number $3,4,6$,and 14, on the upper surface and the nodal coordinates of nodes number $9,10,12$, and 16 on the lower surface, see Fig.7. If the upper and lower surfaces should be divided into more than one element along the span length, Eqn.(21) can be used to calculate the corresponding nodal coordinates. The number of elements along the span length can improve the dynamic simulation results for the design process. Figure (8) shows a tapered wind turbine blade according to NACA 4412 with tapering angle $\alpha = 8^\circ$, the nodes and gradients are illustrated to show the ruled surface between the two edges.

Similar procedure can be carried out to construct the root-blade section with good agreement, see Fig.9. The start cross section of the blade is used with the circular edge of the root surface to construct the lofting surface between them.

## MODELING SLOPE DISCONTINUITY

It is shown in the previous sections, that structural discontinuities are found in two places of the wind turbine blade structure. The first place lies in the interface section between the upper and lower surfaces. These surfaces are generated directly from the NACA code thickness distribution, Eqn.(17), this structural discontinuity can be called as chord-wise slope discontinuity. The second place in the interface between the root-start section and the start-end section of the blade, this structural discontinuity can be called as span-wise slope discontinuity. A method for modeling the slope discontinuities in the wind turbine blade should be described in the following subsections.

### Modeling Chord-Wise Slope Discontinuity

The chord-wise slope discontinuity can be modeled with reasonable accuracy using fillets which can be introduced systematically using initially curved elements. Regarding to Fig.7, a fillet can be used and curved plate elements can be constructed in the leading and trailing edges. In this investigation, a polynomial is established by fitting the points between node number (7) and node number (1) respectively. The order of polynomial depends on the required actuary of the output profile. Using the resulted polynomial, the nodal positions and gradients are estimated at the 'start' and 'end' cross sections of the wind turbine blade. By the fillet constructed on the leading edge of the blade, a continuous structure ANCF model can be constructed. This fillet cancel two nodes, which have the discontinuous gradients. Similar procedure can be used in the trailing edge, and two other nodes should be canceled. By this method, only 12 nodes and 6 plate elements can model the wind turbine blade with a good agreement with the NACA code profile, see Fig.10.

### Modeling Span-Wise Slope Discontinuity

The span-wise slope discontinuity can be modeled by using the lofting equation for the gradients transformation as well as the nodal position transformation. Equation (21) can be used to get the gradients at the lofted cross section. The gradients of the lofted surface can be obtained as:

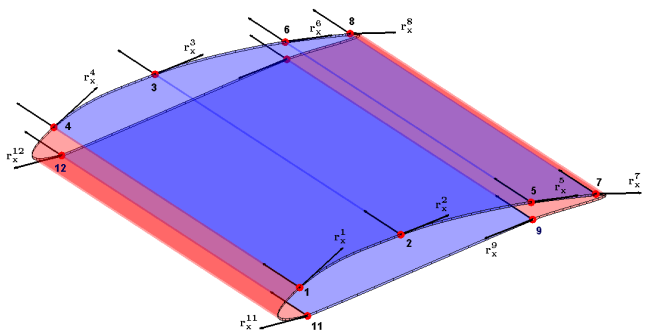

**FIGURE 10**. USING FILLETS AT THE LEADING AND TRAILING EDGES

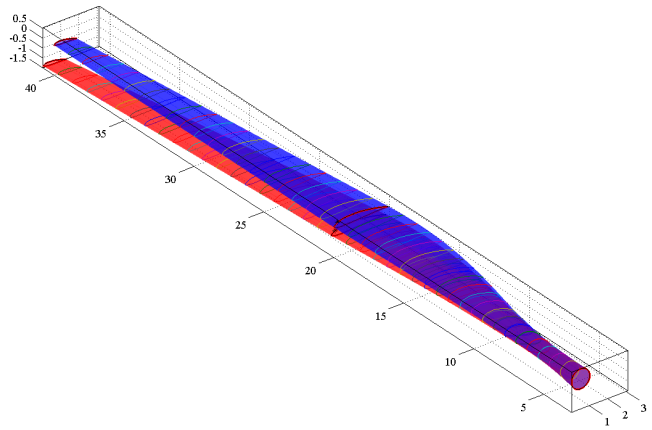

**FIGURE 11**. DYNAMIC SIMULATION DUE TO GRAVITY

$$\frac{d\mathbf{r}(\xi,\eta)}{d\xi} = (1-\eta)\frac{d\mathbf{S}(\xi,0)}{d\xi}\mathbf{e} + \eta\frac{d\mathbf{S}(\xi,1)}{d\xi}\mathbf{e} \qquad (24)$$

$$\frac{d\mathbf{r}(\xi,\eta)}{d\eta} = -\mathbf{r}(\xi,0) + \mathbf{r}(\xi,1) \qquad (25)$$

By using Eqn.(24, 25), a continuous structure ANCF model can be obtained for large-size wind turbine blades. It should be mentioned here that, using Eqn.(24, 25) reduce Eqn.(13) to the identity matrix, and therefore the desirable features of the ANCF can be maintained, as described in section (2).

## DYNAMIC SIMULATION

The dynamic simulation of a cantilevered wind turbine blade is carried out using multibody system computer code, SAMS(Systematic Analysis of Multibody Systems) [30]. The gravity force is introduced as element/nodal forces. The ANCF

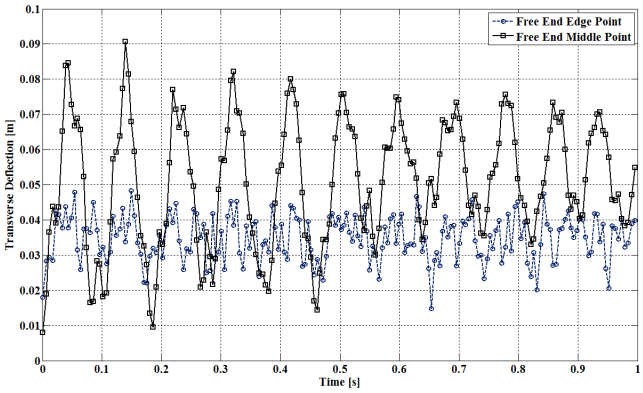


**FIGURE 12**. TRANSVERSE DEFLECTION OF EDGED POINTS ON THE TIP END

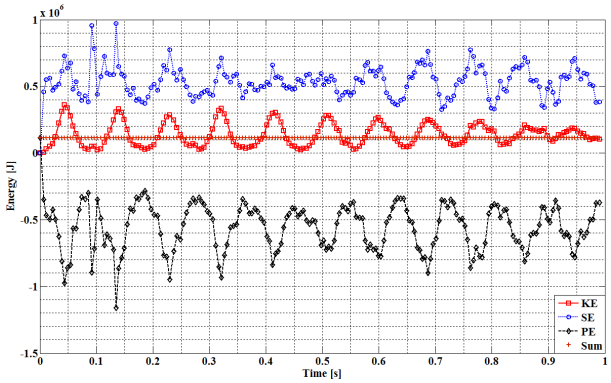


**FIGURE 13**. ENERGY AND WORK BALANCE

of wind turbine blade is constructed using 12 thin plate elements along the blade. The wind turbine blade considered have the following specifications: NACA Code: 4412, chord length $c_1 = 3\,[m]$, span length $L_s = 40\,[m]$, root radius of $0.5[m]$, taper angle $\alpha = 5^\circ$, plate thickness $t = 6\,[mm]$, modulus of elasticity of $200\,[MPa]$, poisson ration 0.33, density 7050 $\left[Kg/m^3\right]$. The numerical integration is carried out by using the sparse HHT integrator [16], with the following parameters: relative and absolute error of $1\times10^{-6}$, constraint tolerance:$1\times10^{-8}$. Figure(11) shows two frames of the dynamic simulation of the moving blade. The transverse deflection of two points on the tip end are plotted in Fig.12, the results shows a numerical convergence in the case of use all deformation modes. It should be mentioned here that the viscoelastic model is quite faster than the elastic model. The energy terms are plotted in Fig.13 which shows a good conservative property of the proposed elastic model.

In the second example, the blade is subjected to air stream with velocity of $3[m/s]$. It is shown by [31] that the aerodynamics characteristics of NACA 4412 are as follows: mid-blade lift coefficient is 1.35 at flow angle of 12.5°, and drag coefficient of 0.03. Other values of the coefficients along the mid-line

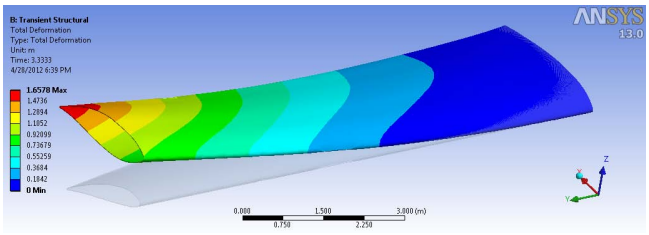


**FIGURE 14**. TRANSIENT RESPONSE OF AERODYNAMIC FORCES WITH ANSYS

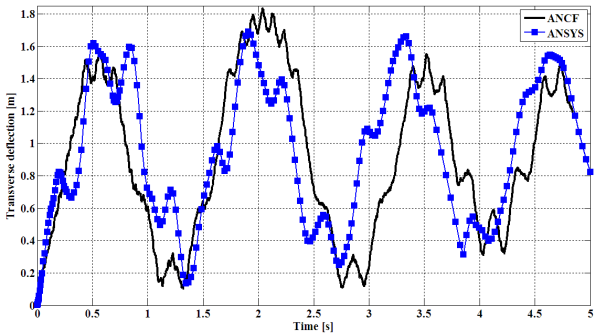


**FIGURE 15**. COMPARISON OF AERODYNAMICS RESPONSES

of the blade are obtained from Ref. [33, 34]. In order to compare the ANCF results with ANSYS, advanced coupled numerical method of computational fluid dynamics (CFD) module and computational flexible multibody dynamics (CFMBD) module has been developed in order to investigate the aero elastic response of this example. The meshing domains of both the blade wall and fluid is established and the ANSYS result is shown in Fig.14. The comparison between the transient responses of the ANCF and ANSYS-FEM models is shown in Fig.15, the numerical results are in good agreement with a noticeable errors due to the non-conforming structure of the reference configuration of the plate elements.

## SUMMARY AND CONCLUSIONS

In this paper, an efficient procedure is developed for mapping NACA airfoil wind turbine blades into absolute nodal coordinate formulation (ANCF) models. The procedure concerned the wind turbine blade with the non-uniform configuration. The structural slope discontinuity due to variations of the cross sectional layouts across the blade is manipulated successfully. The chord-wise slope discontinuity is modeled with reasonable accuracy using fillets which can be introduced systematically using initially curved elements. The span-wise slope discontinuity is modeled by using the lofting surface geometry for the gradients transformation as well as the nodal position transformation. SAMS software package is used for dynamic simulation of the developed blade model. The simulation results show a numerical convergence and satisfy the principle of work and energy in dynamics. Since the ANCF is suited for large-deformation, large-rotation problems, which is the case of large blades, i.e., the use of ANCF opens opportunities to improve the design process of such blades. This work is considered as a necessary step in the Dynamics for Design (DFD) process concerning large-rotation, large-deformation wind turbine blades.

## ACKNOWLEDGMENT

We are grateful to Dynamic Simulation Lab, University of Illinois at Chicago, for generous support of license agreement of SAMS2000 software package and technical support.

## REFERENCES

[1] Kalleoe, B. S., 2007. ”Aeroservoelasticity of Wind Turbines”, PhD thesis, Dept. of mechanical engineering, Technical University of Denmark.

[2] Povl Brndsted, Hans Lilholt, and Aage Lystrup, 2005. ”Composite Materials for Wind Power Turbine Blades”, Annual Review of Materials Research, Vol. 35, PP:505-538.

[3] Holm-Jorgensen, K., Nielsen, S., 2009. ”System reduction in multibody dynamics of wind turbines”, Multibody System Dynamics, Volume: 21, Issue:2, PP147-165.

[4] Jureczko, M., Pawlak, M., Mezyk, A., 2005. ”Optimisation of wind turbine blades”, Journal of Materials Processing Technology , Volume: 167, Issue:2-3, Publisher: Elsevier, Pages: 463-471.

[5] Dufva, K. and Shabana, A.A., 2005. ”Analysis of Thin Plate Structure Using the Absolute Nodal Coordinate Formulation, IMechE Journal of Multi-body Dynamics”, 219, PP:345-355.

[6] Dufva, K. E., Kerkkänen, K. S., Maqueda, L., and Shabana, A. A., 2007, “Nonlinear dynamics of three-dimensional belt drives using the finite-element method”, Nonlinear Dynamics,Volume 48, Number 4, 449-466.

[7] Wan-Suk Yoo, Jeong-Han Lee, Su-Jin Park, Jeong-Hyun Sohn, Dmitry Pogorelov and Oleg Dmitrochenko, 2004, ”Large Deflection Analysis of a Thin Plate:Computer Simulations and Experiments”, Multibody System Dynamics 11: 185–208.

[8] Daniel García-Vallejo, Hiroyuki Sugiyama, Ahmed A. Shabana, 2005,”Finite Element Analysis of the Geometric Stiffening Effect Using the Absolute Nodal Coordinate Formulation”, Proceedings of IDETC/CIE, ASME 2005 International Design Engineering Technical Conferences & Computers and Information in Engineering Conference,September 24-28, 2005, Long Beach, California USA.

[9] Nada, Ayman and El-Assal, Ahmed, 2012. ”Absolute nodal

coordinate formulation of large-deformation piezoelectric laminated plates", Nonlinear Dynamics, Nonlinear Dynamics, 67(4), pp 2241-2454.

[10] Nada, A. A., Hussein, B. A., Megahed,S.M., Shabana A.A., 2010. "Use of the floating frame of reference formulation in large deformation analysis: experimental and numerical validation". Proceedings of the Institution of Mechanical Engineers, Part K: Journal of Multi-body Dynamic 224, 45-58.

[11] Gerstmayr, J., Shabana, A.A., 2006. "Analysis of thin beams and cables using the absolute nodal coordinate formulation", Nonlinear Dynamics, 45, 109–130.

[12] Garcia-Vallejo D., Mayo J., Escalona, J.L., and Dominguez, J.,2004, "Efficient Evaluation of the Elastic Forces and the Jacobian in the Absolute Nodal Coordinate Formulation", Nonlinear Dynamics, 35(4): p. 313-329.

[13] Bassam A. Hussein, Hiroyuki Sugiyama, Ahmed A. Shabana, 2007. "Coupled Deformation Modes in the Finite Element Absolute Nodal Coordinate Formulation", 12th IFToMM World Congress, Besançon (France), June18-21.

[14] Oleg N. Dmitrochenko, Bassam A. Hussein and Ahmed A. Shabana, 2009. " Coupled Deformation Modes in the Large Deformation Finite Element Analysis: Generalization", Journal of Computational Nonlinear Dynamics, April 2009, Volume 4, Issue 2, (8 pages).

[15] Bassam Hussein, Dan Negrut, Ahmed A. Shabana, 2008. "Implicit and explicit integration in the solution of the absolute nodal coordinate differential/algebraic equations", Nonlinear Dyn 54:283–296.

[16] Bassam A. Hussein, Ahmed A. Shabana, 2011."Sparse matrix implicit numerical integration of the Stiff differential/algebraic equations: Implementation", Nonlinear Dyn 65:369–382.

[17] Sugiyama,H., Escalona, J., and Shabana, A.A., 2003, "Formulation of Three-Dimensional Joint Constraints Using the Absolute Nodal Coordinates. Nonlinear Dynamics", 31:pp.167-195.

[18] Garcia-Vallejo,D., Valverde,J., and Dominguez,J., 2005. "An Internal Damping Model for the Absolute Nodal Coordinate Formulation", Nonlinear Dynamics 42: 347–369

[19] Mohamed, Abdel-Nasser, Shabana, Ahmed, 2011. "A nonlinear visco-elastic constitutive model for large rotation finite element formulations", Multibody System Dynamics, Volume: 26, Issue: 1, PP:57-79.

[20] Shabana, A A, and Mikkola, A M, 2003."Use of the finite element absolute nodal coordinate formulation in modeling slope discontinuity." Journal of Mechanical Design 125.2 PP: 342-350

[21] H Sugiyama and Y Suda, 2007. "A curved beam element in the analysis of flexible multi-body systems using the absolute nodal coordinates", Proceedings of the Institution of Mechanical Engineers, Part K: Journal of Multi-body Dynamics, 221: 219-231.

[22] Hiroyuki Sugiyama, Hirohisa Koyama, and Hiroki Yamashita, 2010. "Gradient Deficient Curved Beam Element Using the Absolute Nodal Coordinate Formulation", J. Comput. Nonlinear Dynam. 5, 021001.

[23] Shabana, Ahmed and Maqueda, Luis, 2008. "Slope discontinuities in the finite element absolute nodal coordinate formulation: gradient deficient elements", Multibody System Dynamics, 20 (3), PP:239-249.

[24] Luis G. Maqueda and Ahmed A. Shabana, 2009. "Numerical investigation of the slope discontinuities in large deformation finite element formulations", Nonlinear Dynamics, 58 (1), PP:23-37.

[25] Ahmed A. Shabana, 2011, "General Method for Modeling Slope Discontinuities and T-Sections Using ANCF Gradient Deficient Finite Elements", J. Comput. Nonlinear Dynam. 6, 024502.

[26] Shabana, A.A., 2010, *Computational Continuum Mechanics*, Cambridge University press,Cambridge, UK.

[27] Dreese, J., 2000.,"Aero Basics and DesignFOIL, User Guide, Capitola, California.

[28] Ralph L. Carmichael, "Algorithm for calculating Coordinates of Cambered NACA Airfoils at Specified Chord Locations", AIAA 2001-5235.

[29] Gerlad Farin, 2001, *Curves and Surfaces for CAGD A Practical Guide* ,Fifth Edition, Morgan Kaufmann Publishers.

[30] Shabana, A.A., 2010, *Computational Dynamics*, Third Edition. John Wiley & Sons, Ltd.

[31] Houghton, E.L. and Carpenter,P.W., 2003, *Aerodynamics for Engineering Students*, Fifth Edition, Butterworth-Heinemann.

[32] ANSYS User's Manual, 2001, Theory, Twelfth Edition, SAS IP, Canonsburg.

[33] HUA,X., Rui GU, JIN,J., LIU,Y., Yi MA, CONG, Q., ZHENG, Y., "Numerical Simulation And Aerodynamic Performance Comparison Between Seagull Aerofoil and NACA 4412 Aerofoil under Low-Reynolds", Advances in Natural Science, Vol 3, No 2 (2010).

[34] Rajakumar, S., Ravindran,D., 2010, "Computational Fluid Dynamics Of Wind Turbine Blade At Various Angles Of Attack And Low Reynolds Number", International Journal of Engineering Science and Technology, Vol. 2(11), PP. 6474-6484.